UDC 621.313.33 https://doi.org/10.20998/2074-272X.2026.1.01

V.I. Milykh

Theory and practice of numerical-field analysis and refinement of electromagnetic and energy parameters in the designs of three-phase induction motors

Introduction. *The paper is devoted to improving the designs of three-phase induction motors (TIMs) based on the application of numerical calculations of their magnetic fields. Considering that the classical system for designing TIMs does not always provide sufficient accuracy of their design parameters, this task is relevant and therefore the developed motors require experimental refinement and additional time and money accordingly.* ***Problem.*** *In classic design of TIMs, magnetic calculations are performed based on magnetic circuit theory. The magnetic circuit of TIMs is divided into conditionally homogeneous sections, on which the magnetic quantities are considered to be distributed evenly, but their real distribution is much more complicated. This approach leads to error in determining the electromagnetic parameters of TIMs and, as a result, inaccuracies in energy, mechanical, thermal, etc. calculations. The* ***goal*** *of the paper is to further develop the existing system for designing TIMs by refining it using numerical-field calculations of electromagnetic and energy parameters.* ***Methodology.*** *The methodology is based on numerical-field verification and refinement of classical design of TIMs. It is strictly deterministic, despite the complexity of linear and nonlinear interrelationships of its structural, electromagnetic, and energy parameters, and therefore it is amenable to adequate algorithmization and programming using iterative calculations. The theoretical foundations of the methodology are reinforced by harmonic analysis of time functions of electromagnetic quantities and a refined determination of the differential leakage resistance of the stator winding. The tool for implementing the methodology is the FEMM program in conjunction with the created Lua scripts.* ***Results.*** *Numerical-field calculations of the electromagnetic and energy parameters of the test TIM developed according to the classical design were performed. This motor has been tested within the synchronous idle and rated load conditions. This demonstrated a sufficiently high efficiency of the provided theoretical and practical foundations of numerical-field calculations and revealed that the TIM project does not meet the declared power and voltage requirement. To reach their nominal values, the method for refining the magnetizing current of the stator winding and the rotor slip is provided.* ***Scientific novelty*** *of this paper is the system of numerical-field calculations of electromagnetic and energy parameters of TIMs, which, in conjunction with the iterative process, ensures its output to the specified nominal stator winding voltage and output power while simultaneously varying the magnetizing current and slip.* ***Practical value.*** *The methodology of numerical-field calculations of TIMs based on the FEMM program and the Lua script is recommended to be integrated into the automated design system for these motors. In addition to verifying and refining the parameters of the designed TIMs, the developed methodology and program can be used to obtain a set of refined operating characteristics in an automated calculation mode.* References 29, tables 5, figures 9.

Key words: **three-phase induction motor, automated numerical-field calculations, magnetic field, FEMM, electromagnetic and energy parameters, verification and refinement of design data.**

Вступ. *Робота присвячена удосконаленню проєктів трифазних асинхронних двигунів (ТАД) на основі застосування чисельних розрахунків їхніх магнітних полів. Така задача є актуальною, зважаючи не те, що класична система проєктування ТАД не завжди забезпечує достатню точність їхніх проєктних параметрів, тому розроблювані двигуні потребують експериментальної доводки і відповідно додаткових витрат часу та коштів.* ***Проблема.*** *При класичному проєктуванні ТАД магнітний розрахунок виконується на основі теорії магнітних кіл. Магнітопровід ТАД розділяють на умовно однорідні ділянки, на яких магнітні величини вважаються розподіленими рівномірно, проте реальний їхній розподіл є набагато складнішим. Такий підхід призводить до похибки визначення електромагнітних параметрів ТАД, і, як наслідок, неточності енергетичних, механічних, теплових тощо розрахунків.* ***Метою*** *роботи є подальший розвиток системи проєктування ТАД шляхом її уточнення за допомогою чисельно-польових розрахунків електромагнітних та енергетичних параметрів.* ***Методика*** *побудована на чисельно-польовій перевірці та уточненні класичного проєктування ТАД. Вона є суворо детермінованою, незважаючи на складність лінійних та нелінійних взаємозв'язків конструктивних, електромагнітних та енергетичних його параметрів,тому піддається адекватній алгоритмізації і програмуванню із застосуванням ітераційних розрахунків. Теоретичні основи методики підсилені гармонічним аналізом часових функцій електромагнітних величин та уточненим визначенням диференціального опору розсіювання обмотки статора. Інструментом реалізації методики є програма FEMM у сукупності зі створеними скриптами Lua.* ***Результати.*** *Виконано чисельно-польові розрахунки електромагнітних та енергетичних параметрів тестового ТАД, розробленого за класичним проєктом. Цей двигун перевірено у межах режимів синхронного неробочого ходу та номінального навантаження. Це показало достатньо високу ефективність наданих теоретичних і практичних основ чисельно-польових розрахунків і виявило, що проєкт ТАД не відповідає заявленим потужності та напрузі. Для виходу на їхні номінальні значення надано шлях уточнення намагнічувального струму обмотки статора і ковзання ротора.* ***Науковою новизною*** *в роботі є система чисельно-польових розрахунків електромагнітних та енергетичних параметрів ТАД, яка у сукупності з ітераційним процесом забезпечує його вивід на задані номінальні напругу обмотки статора і вихідну потужність при одночасному варіюванні намагнічуівального струму та ковзання.* ***Практична цінність.*** *Методику чисельно-польових розрахунків ТАД на базі програми FEMM і скрипту Lua рекомендовано вбудовувати в автоматизовану систему проєктування цих двигунів. Окрім перевірки і уточнення параметрів проєктованих ТАД, за розробленими методикою і програмою можна отримати в автоматизованому розрахунковому режимі сім'ю уточнених його робочих характеристик.* Бібл. 29, табл. 5, рис. 9.

Ключові слова: **трифазний асинхронний двигун, автоматизовані чисельно-польові розрахунки, магнітне поле, FEMM, електромагнітні і енергетичні параметри, перевірка та уточнення проєктних даних.**

Introduction. Three-phase induction motors (TIMs) are diverse and widespread in the technosphere around the world. Their improvement is always relevant and occurs due to various factors, including increasing the accuracy and efficiency of the design system.

One of the productive means of improving the design of TIMs is currently the use of numerical field calculations of their magnetic fields (MFs). For this purpose, the publicly available free code FEMM [1],

which is based on the Finite Element Method (FEM), can be used.

The implementation of this code into the TIM design system is facilitated by its convenient interface and the Lua scripting language integrated into it [1, 2]. It provides the creation of program scripts for the automated construction of physical and geometric models of TIMs, reflecting their design, winding currents and magnetic properties of materials. Based on the calculated MFs, the program scripts determine the electromagnetic, power and energy parameters of the designed TIMs.

At present, a combined computational and research system for the design of TIMs has been developed: first, a TIM design is created using classical design methods, such as [3, 4], and then numerical-field studies of TIM are carried out in order to verify, expand the list and improve its design parameters. The author has carried out a number of such various studies, for example, [5–9], etc. And they were subsequently deepened and improved. Naturally, those studies that were carried out at the previous stages were based on larger assumptions and did not yet take into account the achievements of further developments. Therefore, the task now has been to adjust the specified combined computational research system for the design of TIMs, taking into account the achievements obtained and increasing its accuracy by reducing methodological and computational simplifications and assumptions.

The goal of the work is to further develop the TIM design system by refining it using numerical field calculations of electromagnetic and energy parameters. The FEMM code in conjunction with the created Lua scripts was adopted as the tools to achieve the goal.

Analysis of recent research. It is known that induction motors (IMs) have come a long way in their development, but their intensive research continues, as evidenced by the review of publications provided below, although it is far from exhaustive.

Naturally, there are publications devoted to optimization [10, 11], as well as research on new versions of IMs [12, 13]. For example, in the paper [10], the prediction of IM efficiency is investigated using four optimization algorithms: genetic algorithm (GA), particle swarm optimization (PSO), whale optimization algorithm (WOA) and red fox optimization algorithm (RFO). The algorithms were evaluated based on their convergence behavior, accuracy and experimentally measured efficiency values. In the study [11], the FEM is applied to optimize a single-phase IM. This work focuses on current, torque, efficiency and losses using experimental and simulation methods. In the paper [12], the theoretical basis and tools for further optimization of the design of a shaftless IM with a non-contact suspension are presented. The impact on the starting characteristics of the motor is identified by an analytical method and confirmed by FEM modelling. In the paper [13], a double-squirted rotor cage IM is presented, in which high-temperature superconducting materials and copper rods are embedded in different slots. The paper investigates the influence of the rotor slot structure on the torque, as well as related parameters such as the air gap magnetic flux and torque ripple, etc. The computational models based on FEM are implemented in the Ansys Maxwell software. The study [14] focuses on analyzing the influence of different rotor rod designs and materials on the TIM characteristics also using FEM.

In works [15–17, 8] attention is paid to the improvement and development of the theory of IMs. In [15] it is noted that using FEM it is possible to predict the behavior of electromagnetic fields of TIMs, therefore, numerical modeling based on COMSOL was performed as an early tool for studying the interaction between the distribution of these fields and various parameters. In the article [16] it is noted that 3D and 2D models of the motor were created and a 3D finite element (FE) structure was proposed, and thus a number of motor parameters were obtained. In [17] a new high-precision model of IM modelling based on FEM is proposed. The proposed model allows for fast and accurate modelling of IMs using an inverter circuit model and a control algorithm with high accuracy of reflecting non-ideal characteristics of IMs, such as magnetic saturation, spatial harmonics, asymmetry, etc.

In works [18–20] various parameters and processes in IMs are considered. Thus, in the article [18] a dynamic analysis of a two-phase IM with symmetrical and orthogonal phase windings is provided. Based on the geometric dimensions, a model was created for the FEM analysis using the 2D ANSYS Maxwell software. An analysis of the transient and steady-state processes of the machine currents, electromagnetic torque and speed at idle speed and at full load was carried out. In the article [19] an adaptive neural-fuzzy inference system (ANFIS) is presented as a reliable tool for predicting the reduction of the TIM torque under abnormal conditions. The study identifies the main factors of the reduction, including voltage imbalance, harmonic distortion and temperature increase. In the study [20] a method for calculating electrical and magnetic losses in a single-phase IM with a squirrel-cage rotor and non-uniform stator slots is proposed. The simulation was performed using the FEM and AutoCAD software for modelling of non-symmetrical stator slots. The accuracy of the model results was verified by comparing the rated current, torque and efficiency with the motor data. The aim of the work [8] is to further develop the TIM design system by numerical field calculations of active and reactive resistances of TIM windings in the entire range of slip variation and calculation of its mechanical characteristics. The TIM winding resistances are determined by calculations of MF dissipation using the FEMM code, and in the rotor core – with current displacement.

Considerable attention is paid to the diagnostics of IMs [21–23]. In [21], a method for detecting and diagnosing stator short circuits, rotor core breaks, and eccentricity in large IMs by analyzing the frequency spectrum of the stator current was provided. To study the effects of various fault conditions, a time-stepped FEM simulation was performed on a 2D IM model. This leads to more accurate results than other models, since the design geometry and winding scheme of the machine are reflected. In [22], a FE model was developed to study interturn short circuits of the stator winding. Using the developed FE model, simulations were performed to

understand the behavior of various electrical and magnetic quantities in the time and frequency domains. A prototype machine with short circuits was tested in an experimental setup and the results were compared with simulation and analytical calculations. In [23], it is noted that FEM offers a deep understanding of the fundamental principles and physical operation of the machine. It can model complex topology of magnetic circuits, discrete winding schemes and properties of nonlinear magnetic materials of the machine. It determines various parameters of the machine and can model localized magnetic saturation caused by faults with a high degree of accuracy. This article also provides a literature review on methods for diagnosing faults in IMs using FEM.

There are a number of works, for example [9, 24, 25], which are related to the analysis of active and reactive parameters of the stator winding, the use and improvement of equivalent IM circuits, and their operation. In the article [24], a simplified method for estimating the parameters of the IM T-circuit is described, which is based on their design data and on the interaction of numerical and analytical dimensionless approaches using Thevenin theorem. The work [25] provides an estimate of the electrical and mechanical parameters of AC based on the differential evolution algorithm. A comparative study is carried out using different input signals. Such an algorithm is able to estimate the parameters of the equivalent electrical circuit: stator and rotor resistances and leakage inductances, magnetization inductance, and some mechanical parameters. The purpose of the work [9] is to further develop the TIM design system by numerical-field calculation analysis of the differential leakage reactance of the stator winding, as well as a comparative check of the corresponding empirical formulas inherent in the methods of traditional design calculations.

In the article [26], expressions are given for determining the rotor currents of the circular TIM model using field analysis with the existence of spectral harmonics of the stator magnetomotive force. Expressions are developed for determining the winding data and the feasibility of using the calculation model of the sinusoidal stator winding in order to increase the efficiency of mathematical modeling using the equivalent field model with a fixed rotor and slip frequency using the circular model.

The aim of the work [27] is to develop and verify a method for taking into account, using a weakly coupled circuit-field model, the effect of current displacement in the rotor circuit of an induction motor with a squirrel-cage rotor and an IM with massive ferromagnetic elements of the rotor magnetic circuit. The research method consists in iteratively solving the equations of the loop and field mathematical model by refining the parameters of the IM equivalent circuit based on the results of field analysis and in iteratively adjusting the calculated electromagnetic torque to take into account the effect of current displacement obtained on the basis of equivalent currents in the conductive parts of the rotor. The proposed approach makes it possible to increase the reliability of the results of modeling electromagnetic processes in IMs in starting modes.

It can be summarized that the mentioned scientific publications are devoted to various aspects of the development and research of IMs. And it can be noted that a common research tool is numerical calculations of magnetic fields by FEM using various software products. At the same time, this contributes to the improvement of engineering education: the integration of this method for the study of the efficiency of IMs. This is what the article [28] focuses on the implementation of FEM into the engineering curriculum.

A similar modern approach, that is, the use of FEM for the study and improvement of TIMs, is adopted in this article. But here we consider a relevant aspect that has not yet been sufficiently reflected in the scientific literature. Namely, this concerns the problem of numerical-field analysis and refinement of electromagnetic and energy parameters in TIM projects and their verification in principle.

True, there is a work [5] in which this question is raised. But it did not fully reveal this problem, so here this topic is considered in a more complete volume, taking into account the updated system of knowledge and capabilities. Moreover, the work is structured in such a way as to provide TIM researchers with all the opportunities to use the acquired experience of theoretical and practical skills for independent assimilation and application of the presented material.

The object for demonstrating the research performed is the TIM with a short-circuited rotor winding designed in [4], which has a nominal power P_N = 15 kW and a rotation axis height of 160 mm. The main design data of the motor also include the nominal phase voltage U_{sN} = 220 V, the nominal phase current of the stator winding I_{sN} = 28.8 A, the frequency f_s = 50 Hz, the slip s_N = 0.0261 and the power factor $\cos\varphi_{sN}$ = 0.889. The motor has the number of pole pairs p = 2 and the number of phases m_s = 3. The main dimensions include the outer cores diameters of the rotor d_r =184 mm and the stator d_{se} = 272 mm and their length l_a =130 mm, air gap δ = 0.5 mm. The stator has Q_s = 48 slots, the rotor – Q_r = 38 slots. The stator winding is single-layer, diametrical, distributed. The rotor slots are made closed and without bevel. The core material is steel grade 2013.

For numerical field studies using the FEMM code, a 2D computational model was adopted, which is given in Fig. 1 and reflects its electromagnetic system in cross section.

The computational model of the TIM is automatically converted into a physical-geometric model by the created Lua script, as explained in [7]. The geometric model presents the design of the TIM, the physical model carries the distribution and directions of currents in the windings, as well as the magnetic properties of the cores. In Fig. 1, the phase zones of the stator winding are highlighted, which are indicated by phase current labels.

The FEMM code adopts a rectangular coordinate system x, y, but additionally uses polar coordinates r, α. The directions of the rotor rotation frequencies n and of the MF n_s coincide with the direction of the coordinate α.

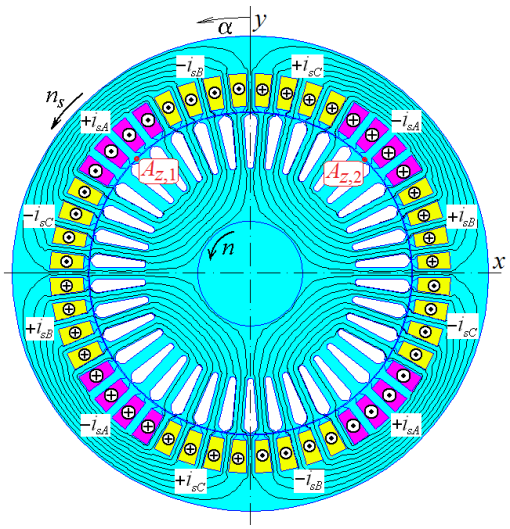

Fig. 1. TIM electromagnetic system with current distribution in the stator winding and the pattern of the lines of force of its magnetic field in the synchronous idle mode

Preparation of the magnetization curve of the TIM core material. On the way to calculating the MF of the TIM by the FEMM code, it is important to set the magnetization curves of the electrical steel from which its cores are made. This, at first glance, trivial task should be performed with an understanding of its essence.

In classical design, the magnetic calculation of the TIM is performed on the basis of the theory of magnetic circuits (TMC). That is, the magnetic core is divided into homogeneous sections, and within each, the magnetic quantities are assumed to be the same. To reduce the error, to take into account its heterogeneity, the main magnetization curve (MMC) of the electrical steel is replaced by special curves – different for the teeth and backs of the cores [3, 4].

Changes in the magnetization curves occur very significantly, as shown in Table 1. For MMC of the steel grade 2013, GOST 21427-83 provides the values of magnetic flux density (MFD) B and magnetic field strength (MFS) H at five reference points. At the same values of the magnetic flux density for the teeth and backs of the cores, the values of H of special curves used in the design methods of TIMs are presented [3, 4]. The differences are obvious.

Table 1

Parameters of magnetization curves of steel 2013

B, T		1,54	1,65	1,75	1,85	2,05
H, A/m	Main	1000	2500	5000	10000	30000
	Teeth	763	990	1330	1770	4400
	Back	608	940	1500	2811	14390

Therefore, the question arises – which magnetization curve should be used in numerical field calculations of TIMs? It is logical to use MMC, because in such calculations the distribution of MFD and MFS in the cores is already inhomogeneous.

Test calculations of the magnetic field by the FEMM code in the synchronous idle mode. In the classical design system, the magnetic calculation of the TIM, as noted, is performed on the basis of the TMC. According to its terminology, this is a straightforward task: the magnetizing current of the motor I_μ is calculated based on a given magnetic flux, which is set in the three-phase stator winding. And this is done without the participation of the rotor winding currents, which is called the synchronous idle mode (SIM) [3, 4].

In general, the article is aimed at identifying the shortcomings of the classical design of the TIMs, which arise due to the use of the TMC for electromagnetic calculations. Therefore, the main assumptions on which the classical design is based are retained in the article in order to concentrate on achieving its specific goal and to identify the role of the TMC in the insufficient accuracy of the calculation of electromagnetic quantities. That is, in this article, by analogy, the sinusoidal nature of the rotor and stator currents is assumed, which is common in many publications, although they note that these currents may have a complicated harmonic composition.

Numerical-field calculation using the FEMM code can verify the adequacy of the calculation of the SIM mode, but such a problem, using the same terminology, is the reverse: the magnetizing current I_μ is set in the stator winding, and the MF is calculated, and on its basis – a number of other electromagnetic parameters of the TIM.

The currents in the phase zones of the stator winding (Fig. 1) are given as for a three-phase symmetrical system:

$$i_{sA} = I_{ms}\cos(\omega_s t);\quad i_{sB} = I_{ms}\cos(\omega_s t - \tfrac{2}{3}\pi);$$
$$i_{sC} = I_{ms}\cos(\omega_s t + \tfrac{2}{3}\pi), \qquad (1)$$

where $I_{ms} = \sqrt{2}\cdot I_s$ is the amplitude of currents; I_s is their effective value; $\omega_s = 2\pi f_s$ is the angular frequency; t is the time.

In the model in Fig. 1, the values of phase currents are given by (1) for the initial time $t = 0$, and then their instantaneous values: $i_{sA} = I_{ms}$, $i_{sB} = i_{sC} = -0.5I_{ms}$. This is the indicated instantaneous directions, which are set according to the indicated conditional positive directions. That is, the signs «+» or «–» before the symbols of the currents are also added to their indicated instantaneous values.

As is known, in all TIM excitation modes, the FEMM code solves a large system of algebraic equations, which are formed on the basis of the FEM and the differential equation describing the MF in the cross section of the TIM electromagnetic system, namely:

$$\mathrm{rot}\left[\frac{1}{\mu(B)}\mathrm{rot}(\vec{k}A_z)\right] = \vec{k}J_z, \qquad (2)$$

where J_z, A_z are the axial components of the current density vector and the magnetic vector potential (MVP); $\vec{k}$ is the unit vector of the axial axis z; μ is the magnetic permeability: either the magnetic constant μ_0 for non-magnetic areas, or determined for MFD B from the magnetization curve of the material.

The result of solving equation (2) by the FEMM code is the coordinate distribution of the MVP $A_z(x, y)$.

The calculation of the MF was performed at the design magnetizing current of the stator winding I_μ = 7.75 A, the value of which is substituted in (1) instead of I_s. The calculated picture of the MF in the SIM mode is given in Fig. 1.

To compare the design data and the results of numerical-field calculations, the magnetic flux was first taken, which is defined as

$$\Phi_0 = \left(A_{z,1} - A_{z,2}\right) l_a , \qquad (3)$$

where A_{z1}, A_{z2} are the values of the MVP at two points through which the sides of the circuit for which the flux is determined pass.

To determine the magnetic flux at the pole pitch, the points are located in the interval: the first of them is where the MVP has the maximum positive value A_{z1}, the second one is where the maximum negative value A_{z2}. In the SIM mode, the location of these points is shown in Fig. 1.

In this way, we obtained A_{z1} = 34.859 mWb/m; A_{z2} = –34.857 mWb/m and by (3) Φ_0 = 9.063 mWb. This is close enough, although with a clarification: the magnetic flux in the TIM design has a value of 9.005 mWb.

However, if special separate magnetization curves for the stator teeth and backs were used in the numerical-field calculation (see Table 1), then a less acceptable magnetic flux would be obtained Φ_0 = 9.703 mWb (a difference of 7 % is too large).

In the numerical-field calculations of TIMs, magnetic flux linkage (MFL) plays a significant role.

For the phase winding of the stator, which has N_s consecutive turns, according to Fig. 1, the MFL

$$\Psi_s = N_s \cdot l_a \times$$

$$\times \left(\frac{1}{S_1} \int_{S_1} A_z dS - \frac{1}{S_2} \int_{S_2} A_z dS + \frac{1}{S_3} \int_{S_3} A_z dS - \frac{1}{S_4} \int_{S_4} A_z dS \right), \qquad (4)$$

where integration occurs over the cross-sectional areas S_1–S_4 of the conductive part of the slots of the phase zones with the currents markings $+i_{sA}$ та $-i_{sA}$ of the phase winding A.

This MFL is created by a magnetic field on the active length of the cores, i.e. on the slot part of the TIM stator winding. The determination of areas and integrals for (4) in Lua scripts occurs automatically using special functions. And thus the MFL of the stator phase winding Ψ_{ms} = 0.9843 Wb was obtained.

In the position of the phase winding A considered in Fig. 1, this is the maximum value of the MFL, so it is possible to calculate the effective value of the phase EMF

$$E_s = \sqrt{2}\,\pi\, f_s\, \Psi_{ms} = 218{,}7 \text{ V}, \qquad (5)$$

where the winding distribution is automatically taken into account.

In the TIM design, the similar value is 214.5 V, and the existing EMF error, as a result, gives inaccuracies in further design calculations.

The refined calculation of the phase EMF of the stator winding. The considered definition of the MFL and the EMF of the phase winding of the stator can be considered as a first approximation, because the amplitude of the MFL is taken at one position of its phase zones. It is more justified to use a discrete angular function of the MFL on its period.

Specifically, according to the distribution of the MVP in the cross section of the TIM, according to (4), the values of the MFL of the phase winding A are «collected» with a conditional movement of its phase zones in the angular direction. The process of moving of the conditional «mask» of the phase zones in the angular direction along the slot structure of the stator is shown in Fig. 2 (the first three and the last 24th positions are shown).

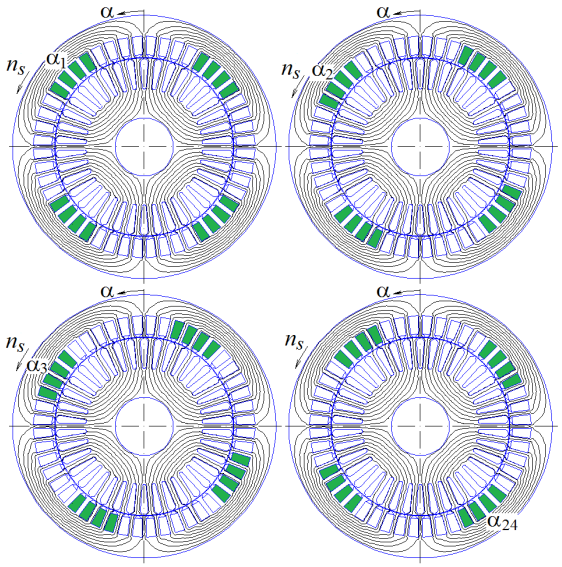

Fig. 2. Movement of the «mask» of the phase zone of the stator winding for collecting the MFL within the period of its angular function against the background of the calculated magnetic field

Thus, the discrete angular numerical function of the MFL appears (Table 2):

$$\Psi_k(\alpha_k); \quad \alpha_k = (k-1)\tau_s; \quad k = 1, 2, 3, \ldots K , \qquad (6)$$

where k is the counter of the positions of the conditionally movable «mask» of the phase zone; $K = Q_s/p$ is the number of such positions within two pole steps τ_p, which is the period of function (6); τ_s=360°/Q_s is the tooth-slot step of the stator core.

Table 2

Angular discrete function of the MFL Ψ_k of the phase winding A at 24 angular positions, Wb

k	1	2	3	4	5	6
Ψ_k	0,9843	0,9430	0,8337	0,6685	0,4617	0,2349
k	7	8	9	10	11	12
Ψ_k	0,0001	–0,2347	–0,4614	–0,6683	–0,8335	–0,9428
k	13	14	15	16	17	18
Ψ_k	–0,9843	–0,9430	–0,8337	–0,6685	–0,4617	–0,2349
k	19	20	21	22	23	24
Ψ_k	–0,0001	0,2347	0,4614	0,6683	0,8335	0,9428

The angular function (6) is converted into a time function by the relationship $\alpha = \Omega_s t$, where $\Omega_s = \omega_s/p$ is the angular velocity of the TIM rotating magnetic field. The time function obtained in this way preserves the values of the MFL according to Table 2, and it is depicted in Fig. 3 (curve 1).

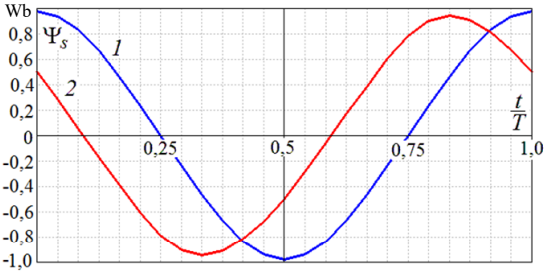

Fig. 3. Time function of the MFL of the stator phase winding within its period T: 1 – synchronous idle mode; 2 – nominal load

The function $\Psi_s(t)$ is periodic, therefore it is decomposed into a harmonic Fourier series on its period in two pole steps (Fig. 3), on which the MFL is calculated at K points (in this TIM $K = 24$).

Considering that cosine functions (1) are taken for the stator winding currents, a harmonic series of similar functions is determined for the MFL, i.e. a harmonic time function is obtained, which corresponds to a stationary phase winding A:

$$\Psi = \sum_{\nu=1,3,5...}^{N_g} \Psi_{m\nu} \cos(\nu \omega_s t + \gamma_{\psi\nu}), \qquad (7)$$

where the amplitudes of $\Psi_{m\nu}$ and the arguments of $\gamma_{\psi\nu}$ (initial phases) of the harmonics ν are determined by well-known mathematical rules, which was shown in [6, 9] and other works.

It is known that the number of the highest harmonic N_g cannot exceed $K/2$. In (7) the values of $\nu\omega_s t$ and $\gamma_{\psi\nu}$ are measured in electrical radians or degrees.

From the MFL function (7) based on the law of electromagnetic induction by the expression $e = -d\Psi/dt$ we proceed to the harmonic time function of the EMF of the phase winding:

$$e_s = \sum_{\nu=1,3,5...}^{N_g} \nu\omega_s \Psi_{m\nu} \cos\left(\nu \omega_s t + \gamma_{\psi\nu} - \pi/2\right), \qquad (8)$$

where the amplitudes of the ν-th EMF harmonic are separated

$$E_{m\nu} = \nu\omega_s \Psi_{m\nu} \qquad (9)$$

as well as its corresponding initial phase

$$\gamma_{E\nu} = \gamma_{\psi\nu} - \pi/2 . \qquad (10)$$

Also, according to the known relationship for harmonic functions, the effective value of the EMF of the ν -th harmonic is obtained through the amplitude, namely:

$$E_{s\nu} = \sqrt{2}\pi f_s \nu \Psi_{m\nu} . \qquad (11)$$

Time functions (7) and (8) in Table 2 and Fig. 3, respectively, have a semi-periodic asymmetry:

$$\Psi_{s,k}(\alpha_k) = -\Psi_{s,k}(\alpha_k + \tau_p);\ k = 1, 2, 3, ... K , \qquad (12)$$

therefore, their harmonic series contain only odd harmonics, i.e. for these functions we get $N_g = 11$.

Taking into account the entire harmonic composition, we find the equivalent effective value of the phase EMF of the stator winding

$$E_{seq} = \sqrt{\sum_{\nu=1,3,5...}^{N_g} E_{s\nu}^2} . \qquad (13)$$

The considered method was transformed into a Lua script, which was combined with the calculation of the MF using the FEMM code, and as a result the following results were obtained: amplitude and initial phase of the first harmonic of the MFL $\Psi_{m1} = 0.9630$ Wb; $\gamma_{\psi 1} = 0$, effective value and initial phase of the first harmonic of the phase EMF $E_s = 213.9$ V, $\gamma_{Es} = -\pi/2$; effective value of the total EMF according to (13) $E_{seq} = 214.3$ V.

The harmonic composition of the MFL (7) and EMF (8) in relative units (p.u.) is given in Table 3 (take the values of their first harmonics as the basis), and the effective values of the EMF harmonics $E_{s\nu}$ according to (11) are also given.

Table 3

Harmonic composition of MFL and EMF in the SIM mode

ν	–	1	3	5	7	9	11
$\Psi_{m\nu}$	p.u.	1,000	0,0203	0,0003	0,0010	0,0009	0,0002
$E_{m\nu}$	p.u.	1,000	0,0610	0,0013	0,0067	0,0078	0,0027
$E_{s\nu}$	V	213,9	13,04	0,29	1,44	1,66	0,58

Note that here and after that there are harmonics, multiples of three, which supposedly contradicts the classical theory of three-phase electric machines. But this theory is built on the step functions of the distribution of the MMF of the stator winding under the conditions of a toothless rotor and a completely unsaturated magnetic circuit. Under such conditions, the numerical-field calculation and formulas (7), (8) also gave zero third harmonics as well as multiples of it. However, when the magnetic circuit and, first of all, the stator teeth are saturated, these harmonics appeared, and in the load mode, the presence of current in the rotor winding also contributes to such harmonics. The specified features of the harmonic composition are also confirmed in work [29] on the example of a three-phase stator winding of a turbogenerator.

And another significant difference between the classical harmonic analysis methods and the one used in the article is that the first is done according to the conditional stepwise distribution of the MMF and magnetic flux density in a «smooth» interval (in reality, this is nowhere near the case), and the second is done according to the MFL of the winding directly in the slots, taking into account the real geometry of the TIM electromagnetic system and core saturation.

Refining of the magnetizing current of the stator winding. To determine the balance of voltages in the electric circuit of the stator winding and further clarify the magnetizing component of its current, the voltage equilibrium equation in vector form is useful:

$$\underline{U}_s = -\underline{E}_s + \underline{U}_{Rs} + \underline{U}_{s\sigma dif} + \underline{U}_{s\sigma fh} , \qquad (14)$$

where the vectors are applied: EMF $\underline{E}_s$; voltage drop across the active resistance of the stator winding $\underline{U}_{Rs}$ and across the inductive resistances of its differential $\underline{U}_{s\sigma dif}$ and frontal $\underline{U}_{s\sigma fh}$ dissipation (the inductive resistance of the slot dissipation is already taken into account in the EMF $\underline{E}_s$ due to the definition of the full MFL of the stator winding (4) within its active part along the length of the TIM cores); the stator winding current vector has a zero initial phase according to (1).

The phase relations of the quantities with (14) are illustrated in Fig. 4 by a vector diagram (VD) of a general form (without observing the scale of the vectors, because it will be used in different calculation modes). We also note that equations (14) and VD in Fig. 4 correspond to the first harmonics of the quantities, because they are also used in TIM designs.

The inverted EMF vector $-\underline{E}_s$ is shifted by an angle $\varphi_{Es} = 180° + \gamma_{Es}$ with respect to the current, and it has the effective values of the active and reactive components: $E_{sa} = E_s\cos\varphi_{Es}$; $E_{sr} = E_s\sin\varphi_{Es}$. The effective values of the voltage drops on the specified resistances are calculated by the formulas $U_{Rs} = R_s I_s$; $U_{s\sigma dif} = X_{s\sigma dif} I_s$; $U_{s\sigma fh} = X_{s\sigma fh} I_s$. These resistances are determined when designing the TIM

and have the values R_s= 0.402 Ω, $X_{s\sigma dif}$ = 0.253 Ω; $X_{s\sigma fh}$ = 0.234 Ω.

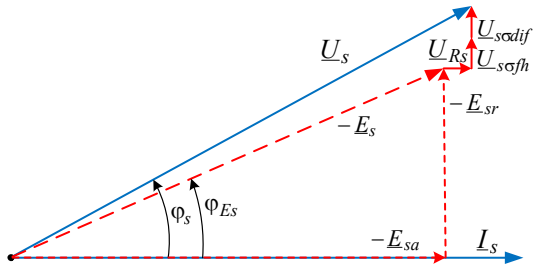

Fig. 4. Vector diagram of voltages in the stator phase winding

Through the components of the vectors according to equation (14) and Fig. 4, the active and reactive components of the phase voltage $\underline{U}_s$ are obtained:

$$U_{sa} = E_{sa} + U_{Rs}\,;\quad U_{sr} = E_{sr} + U_{s\sigma dif} + U_{s\sigma fh}\,,$$

as well as its effective value and phase shift relative to the current $\underline{I}_s$:

$$U_s = \sqrt{U_{sa}^2 + U_{sr}^2}\,;\quad \varphi_s = \text{arctg}(U_{sr}/U_{sa})\,.$$

Considering the SIM mode, it is necessary to substitute the corresponding current I_μ everywhere instead of I_s.

Substitution of all values into the above formulas gives an effective voltage value of 217.7 V, which does not «reach» 220 V, that is, the nominal U_{sN}.

Therefore, to reach the nominal voltage of the stator winding, an iterative search for the corresponding magnetizing current was used.

In this way, after three iterations, the refined value of this current I_μ = 8.09 A was determined, and the values of the remaining quantities mentioned were Ψ_{m1} = 0.9725 Wb; E_s = 216 V, U_{Rs} = 3.3 V; $U_{s\sigma dif}$ = 2 V; $U_{s\sigma fh}$ = 1.9 V; U_s = 220 V.

Additionally, the ratio of the phase voltage to the phase EMF of the stator winding was obtained during synchronous rotation of the rotor and the TIM magnetic field

$$k_{UE} = U_s / E_{ss} = 1{,}028\,, \qquad (15)$$

where $E_{ss} = \sqrt{E_{sa}^2 + (E_{sr} - U_{s\sigma n})^2}$ =214.1 V is the phase EMF without all dissipation components, $U_{s\sigma n}$= $X_{s\sigma n}I_s$ = = 1.9 V is the voltage drop across the slot leakage reactance; E_{sa} = 0; E_{sr} = 216 V is the active and reactive components of EMF E_s (in the SIM mode, according to calculations, φ_{Es} = 90° was turned out).

The value of k_{UE} is important for further calculation of the TIM loading mode (in the design from [4] its value is 1.026).

Calculations of the TIM magnetic field in its loading mode. For this mode, a strictly deterministic interconnected system of stator and rotor currents is required. The calculation model of the TIM with the system of these currents is given in Fig. 5.

The angular positions of the rotor slots are fixed by the coordinate of the first slot α_{r1}, which is closest to the left to the y axis (in Fig. 5 α_{r1} = 0). The remaining slots are numbered by the counter k and they are shifted from each other by the angle of the rotor tooth pitch $\alpha_{rn} = 360°/Q_r$.

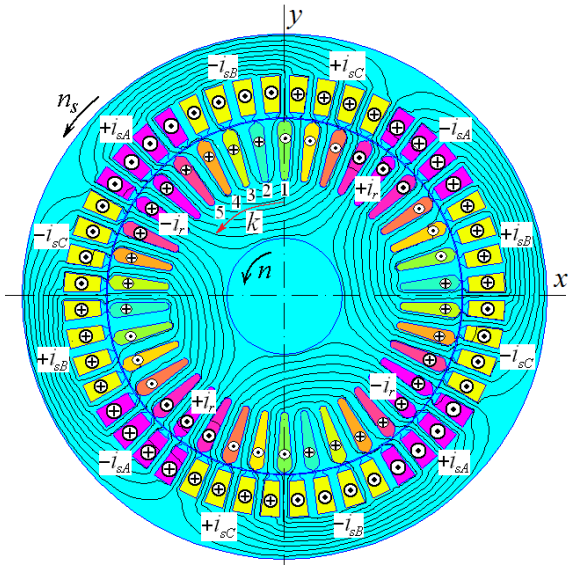

Fig. 5. Distribution of currents in the TIM windings in the rated load mode and the corresponding picture of the power lines of the MF

For calculating the TIM MF in the loading mode, the key is to set the corresponding currents in the windings, taking into account the phase shift between them. For their determination, calculations are used according to the formulas that are given below in the text based on [4].

The basis of such calculations is the slip s, for which its design value s_N is initially given, as well as the magnetizing current of the stator winding I_μ, which is determined in the SIM mode. But then their values are refined.

The SIM mode current I_{sos} has a reactive component I_{srs}, which is practically equal to I_μ, as well as an active component I_{sas}, which is determined under the condition $I_{sas} \ll I_\mu$:

$$I_{sas} = \frac{P_{mags} + m_s R_s I_\mu^2}{m_s U_s}\,, \qquad (16)$$

where P_{mags} are the magnetic losses in the stator core.

The currents in the phase zones of the stator winding in Fig. 5 are determined by the formulas of their symmetrical system (1) and are distributed as in the SIM mode (Fig. 1).

To determine the rotor currents and explain their distribution over the slots, the L-shaped equivalent circuit of the TIM (Fig. 6) [4] and the corresponding VD, which is constructed in Fig. 7, are used. The basic one is the phase current vector $\underline{I}_s$, which, according to (1), has a zero initial phase.

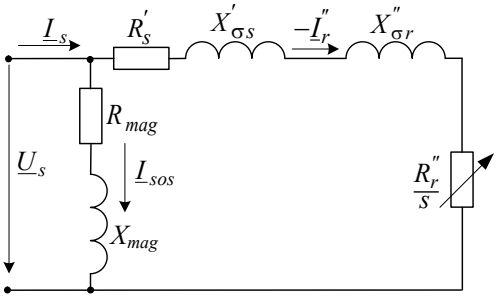

Fig. 6. Converted L-shaped equivalent circuit of the reduced IM

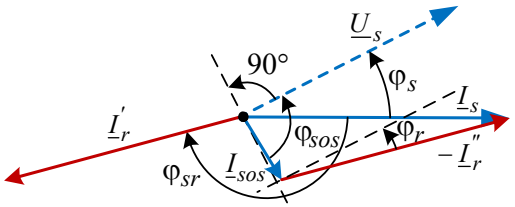

Fig. 7. Vector diagram of phase relations of TIM winding currents

Important for calculating currents and other electromagnetic parameters of the TIM are the active and reactive resistances of its windings. They are reflected in the equivalent circuit, and their values are found during design. To the already given values of the stator winding resistances R_s, $X_{s\sigma dif}$; $X_{s\sigma fh}$ we add the total reactance of its dissipation $X_{\sigma s} = 0.725$ Ω.

For a short-circuited rotor winding, the active resistance on its phase part is $R_r = 53.9 \cdot 10^{-6}$ Ω. This active resistance $R'_r = 0.196$ Ω and the leakage reactance $X'_{\sigma r} = 1.02$ Ω reduced to the stator winding are also used.

Reactance of the magnetizing branch of the equivalent circuit:

$$X_{mag} = U_{sN} / I_\mu - X_{\sigma s}, \qquad (17)$$

active resistance $R_{mag} << X_{mag}$ due to condition $I_{sas} << I_\mu$.

All of the indicated resistances for the equivalent circuit (Fig. 6) have an additional transformation:

$$X'_{\sigma s} = c_1 X_{\sigma s};\ R'_s = c_1 R_s;\ X''_{\sigma r} = c_1^2 X'_{\sigma r};\ R''_{\sigma r} = c_1^2 R'_r,$$

where $c_1 = 1 + X_{\sigma s} / X_{mag}$ is the coefficient characterizing the ratio of the voltage vector to the EMF vector of the stator winding during synchronous rotation of the rotor – this is an analogue of the coefficient k_{UE} (15).

Based on the design data of the TIM and in accordance with the equivalent circuit of the combined TIM (Fig. 6) and the VD (Fig. 7), the reactive and active resistances of the load branch:

$$X_{rs} = c_1 (X_{\sigma s} + c_1 X'_{\sigma r});\ R_{rs} = c_1 R_s + c_1^2 R'_r / s. \qquad (18)$$

The rotor current of such a motor and its phase shift with respect to the stator winding voltage U_s

$$I''_r = \frac{U_s}{\sqrt{R_{rs}^2 + X_{rs}^2}};\ \varphi_r = \operatorname{arctg}(X_{rs} / R_{rs}), \qquad (19)$$

and then the effective value of the real (not reduced) rotor winding current

$$I_r = c_1 I''_r K_{Isr}, \qquad (20)$$

where the reduction factor of the rotor winding current to the stator winding current [3]

$$K_{Irs} = \frac{N_s K_{Ws} m_s}{N_r K_{Wr} m_r} \cdot \frac{1}{K_{sq}}, \qquad (21)$$

which includes $N_s = 112$ – the number of consecutive turns in the phase winding of the stator; $K_{Ws} = 0.959$ – its winding coefficient; for a short-circuited rotor winding, the number of phases $m_r = Q_r$, and for each number of turns $N_r = 0.5$, the rotor winding coefficient $K_{Wr} = 1$; the bevel coefficient of its slots $K_{sr} = 1$.

Based on the above, the reactive and active components of the stator phase current are obtained

$$I_{sr} = I_\mu + I''_r \sin\varphi_r;\ \ I_{sa} = I_{sas} + I''_r \cos\varphi_r, \qquad (22)$$

then its effective value and phase shift angle relative to the phase voltage U_s:

$$I_s = \sqrt{I_{sa}^2 + I_{sr}^2};\ \ \varphi_s = \arccos(I_{sa} / I_s). \qquad (23)$$

Thus, according to the VD (Fig. 7), the electrical phase shift angle between the currents I_s and I_r (in degrees) is obtained:

$$\varphi_{sr} = 180° - \varphi_s + \varphi_r, \qquad (24)$$

which in the motor design is converted into a geometric angle

$$\alpha_{sr} = \varphi_{sr} / p. \qquad (25)$$

On the basis provided, a multiphase system of instantaneous current values in the rods of the short-circuited rotor is formed, namely:

$$i_{rk} = I_{mr} \sin\left\{p \cdot \left[\beta + (k-1) \cdot \alpha_{rn} + \alpha_{sr} + \alpha_{r1}\right]\right\}, \qquad (26)$$

where $k = 1, 2, \ldots, Q_r$ is the numbering of the rotor slots adopted in Fig. 5; $I_{mr} = \sqrt{2} \cdot I_r$ is the amplitude of the phase current in the rotor rods; β=0 is the initial phase of stator current.

The calculations yielded the following values: $I_s = 28.8$ A; $\varphi_s = 27.25°$; $\varphi_r = 12.23°$; $\varphi_{sr} = -164.98°$; $K_{Irs} = 16.9$; $I_r = 446$ A; $\alpha_{sr} = -82.49°$.

The distribution of currents along the slots of the stator and rotor at pole pitches τ_p in dimensionless form is shown in Fig. 8 (the indicated points are meaningful for the currents, the lines are drawn for their visual connection).

In accordance with the presented methodology and the design parameters of the TIM in the nominal load mode, its MF was calculated. The distribution of currents in the TIM slots and the MF picture calculated by the FEMM code are given in Fig. 5.

According to the calculated MF, a number of TIM parameters were determined using the same method as for the SIM mode.

The magnetic flux in the gap per pole pitch according to the formula (3) $\Phi_l = 8.781$ mWb, i.e. it turned out to be 3.1 % less than in the SIM mode.

The time function of the MFL of the stator phase winding in the nominal mode is shown in Fig. 3 (curve 2) in comparison with the similar function in the SIM mode.

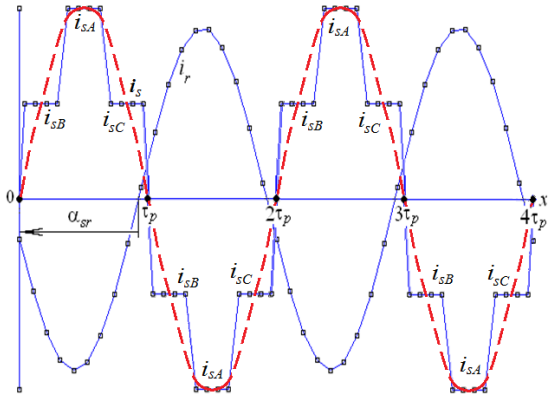

Fig. 8. Angular discrete distributions of winding currents of the rotor i_r and stator i_s of the TIM along its slots on the sweep of the circular line passing through the gap

Table 4 gives the harmonic composition of the time functions of the MFL Ψ_{mv} and the values of the EMF amplitudes E_{mv} (in relative units), as well as the absolute effective values of the EMF E_{sv} of the stator winding, which can be compared with the data in the similar Table 3 for the SIM mode.

Table 4

Harmonic composition of MFL and EMF in the rated loading mode

ν	–	1	3	5	7	9	11
Ψ_{mv}	p.u.	1,000	0,0216	0,0069	0,0031	0,0001	0,0011
E_{mv}	p.u.	1,000	0,0648	0,0347	0,0217	0,0011	0,0117
E_{sv}	V	206,9	13,41	7,18	4,49	0,23	2,42

Amplitude and initial phase of the first harmonic of the MFL $\Psi_{m1} = 0.9313$ Wb; $\gamma_{\psi 1} = -56.55^\circ$, effective value and initial phase of the first harmonic of the phase EMF $E_{s1} = 206.9$ V; $\gamma_{E1} = 33.45^\circ$; full EMF by (13) $E_{seq} = 207.5$ V; by (17) phase voltage $U_s = 224.7$ V and the phase shift of the current relative to it $\varphi_s = 34.84^\circ$ (Fig. 7); voltage drops $U_{Rs} = 7$ V; $U_{s\sigma dif} = 7.4$ V; $U_{s\sigma fh} = 6.9$ V.

Using all higher harmonics the effective value of the differential EMF of the stator winding is obtained [9]

$$E_{sdif} = \sqrt{\sum_{\nu=3,5...}^{N_g} E_{s\nu}^2} = 16.05 \text{ V}, \quad (22)$$

as well as the refined differential resistance of the stator winding

$$X_{s\sigma dif} = \frac{E_{sdif}}{I_s} = 0.61 \ \Omega. \quad (23)$$

Note that this resistance is found here in compliance with its mathematical and physical essence, as discussed in [9], and it differs significantly from the design value (see above in the text), which is found using the approximate method. Therefore, further calculations will be performed with the updated value $X_{s\sigma dif}$.

In loading mode, the energy parameters of the TIM are important:

- input electrical power of the TIM:

$$P_{in} = m_s U_s I_s \cos\varphi_s ; \quad (24)$$

- electromagnetic torque, which is determined by a special Lua function through Maxwell magnetic tension tensor

$$M_{em} = \frac{l_a}{\mu_0 (r_s - r_r)} \int_{S_\delta} B_r B_\alpha r \mathrm{d}S , \quad (25)$$

where B_α, B_r are the angular and radial components of the magnetic flux density vector; S_δ is the cross-sectional area of the non-magnetic gap; r_r and r_s are the radii of the circles bounding this plane on the sides of the rotor and stator;

- electromagnetic power transmitted by the rotating magnetic field from the stator to the rotor:

$$P_{em} = M_{em} \Omega_s , \quad (26)$$

where Ω_s is the angular velocity of this field which has already been mentioned;

- electrical power losses in the stator and rotor windings

$$P_{els} = m_s R_s I_s^2 ; \quad P_{elr} = m_r R_r I_r^2 . \quad (27)$$

The values of the remaining power losses in these calculations do not change and are taken from the TIM design [4]: P_{mags} – magnetic losses in the stator core, P_{mec} – mechanical losses, additional losses P_{ad}, P_{magr} – magnetic losses in the rotor core, which consist of surface and pulsation losses.

Taking into account the losses related to the rotor, the output useful power of the TIM is determined:

$$P_{out} = P_{em} - P_{elr} - P_{mag\,r} - P_{mec} - P_{ad} . \quad (28)$$

And finally, the efficiency of the TIM:

$$\eta = P_{out} / P_{in} . \quad (29)$$

The mentioned power losses have the following values: P_{els} = 1046 W; P_{elr} = 407.7 W; P_{mags} = 270 W; P_{magr} = 87.3 W; P_{mec} = 117 W; P_{ad} = 84.3 W.

According to the provided formulas, the integral energy parameters of TIM were obtained: $M_{em} = 97.72$ N·m; $P_{in} = 16.667$ kW; $P_{em} = 15.350$ kW; $P_{out} = 14.741$ kW; $\cos\varphi_s = 0.821$; $\eta = 0.884$.

The phase voltage based on (14) U_s = 224.7 V turned out to be greater than the nominal, but the motor should operate at the nominal voltage of 220 V.

To eliminate the excess U_s, it is necessary to reduce the magnetizing current of the stator winding I_μ. Therefore, by iterative method, numerical-field calculations using the provided method found $I_\mu = 7.25$ A, and accordingly, the stator winding current reached $I_s = 29.22$ A. Of course, not only the voltage changed, but also the remaining quantities, which acquired the following values: $\Psi_{m1} = 0.9101$ Wb; $\gamma_{\psi 1} = -57.17^\circ$; $E_{s1} = 202.4$ V; $\gamma_{E1} = 32.83^\circ$; $\alpha_{sr} = 83.10^\circ$; $E_{seq} = 207.5$ V; $U_{Rs} = 7$ V; $U_{s\sigma dif} = 7.4$ V; $U_{s\sigma fh} = 6.8$ V; $U_s = 220$ V; $\varphi_s = 34.28^\circ$; $M_{em} = 95.45$ N·m; $P_{in} = 16.288$ kW; $P_{em} = 14.988$ kW; $P_{out} = 14.379$ kW; $\cos\varphi_s = 0.826$; $\eta = 0.883$.

From all of this, it can be noted that the voltage U_s has become nominal, but the output power P_{out} does not reach the nominal value, which is 15 kW.

It is clear that the task of simultaneously providing nominal voltage and output power is complex, and for its solution, an appropriate method has been developed based on the methodology from [4] and the development of [5].

The complexity of the problem lies in the fact that the input values s, I_μ and the output values U_s, P_{out} are interconnected, that is, it is a four-parameter problem, and therefore it is solved by an iterative method. For this purpose, a strictly deterministic method is provided, the essence of which is described further in the text, and then the results of calculations performed by a program on a Lua script, which provides interaction with the FEMM code, are provided.

Iterative determination of the slip and magnetizing current of the stator winding for simultaneous output to the rated voltage and power of the TIM. For a visual representation of the technique, a graphical model is used, given in Fig. 9. It is based on a coordinate system with the desired parameters: rotor slip s and magnetizing current of the stator winding I_μ.

This coordinate system is represented in axonometry by the plane s, I_μ, in which the point 0 is placed with the coordinates of the slip s_0 and the magnetizing current $I_{\mu 0}$, which are given in the current iteration for calculating the voltage U_s and the power P_{out}.

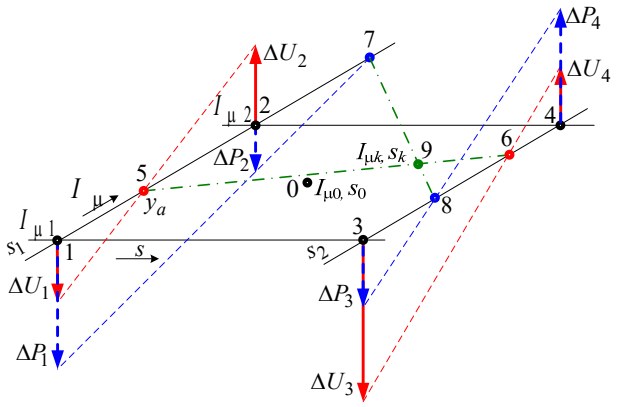

Fig. 9. Diagram of the varying current I_μ and slip s and the deviation of the desired values U_s and P_{out}

In the first iteration, the values of the slip s_0 and the current P_{out} are taken directly from the TIM design [4]. In essence, this is the first approximation of the values of the varied quantities of the iterative process to be performed.

Around the coordinate point s_0, $I_{\mu 0}$ in the specified plane there is a rectangle with reference points 1, 2, 3 and 4. The corresponding lines 1-2 and 3-4 have the slip coordinates s_1 and s_2, lines 1-3 and 2-4 have the current coordinates $I_{\mu 1}$ and $I_{\mu 2}$.

Then the sides of the rectangle have dimensions

$$\Delta s = s_2 - s_1;\ \ \Delta I = I_{\mu 2} - I_{\mu 1}. \qquad (30)$$

These dimensions are chosen such that it is possible to allow within their limits a linear dependence of the voltage U_s and the power P_{out} on the slip s and the current I_μ. For example, for the first iteration, it is possible to set $\Delta s = 0.05 s_0$; $\Delta I = 0.05 I_{\mu 0}$ based on experience of calculations, and then for each subsequent iteration these dimensions are halved.

Thus, in Fig. 9 the coordinates of four points 1-4 are given:

$$s_1 = s_0 - \Delta s/2;\ \ s_2 = s_0 + \Delta s/2;\ \ I_{\mu 1} = I_{\mu 0} - \Delta I/2;\ \ I_{\mu 2} = I_{\mu 0} + \Delta I/2. \qquad (31)$$

For each of the given points (31), the MF calculation is performed in the TIM loading mode. According to the results of these calculations, the corresponding values of the phase voltage U_s (14) and the output power P_{out} (28) are determined at these points using the method given above:

$$U_{s,k};\ P_{out,k},\ k = 1, 2, 3, 4, \qquad (32)$$

as well as the mismatches of these quantities relative to their nominal values:

$$\Delta U_k = U_{s,k} - U_{sN};\ \Delta P_k = P_{out,k} - P_N,\ k = 1, 2, 3, 4. \qquad (33)$$

The specific coordinates of the points according to (31) and the values of the mismatch of the phase voltage U_s and the output power P_{out} according to (33) are given in Table 5.

Table 5

Mismatches of values on the first iteration

Variation	$s_1 = 0.0248$	$s_2 = 0.0274$
$I_{\mu 1} = 6.849$ A	$\Delta U_1 = -2.59$ V $\Delta P_1 = 1311$ W	$\Delta U_3 = -3.17$ V $\Delta P_3 = -218$ W
$I_{\mu 2} = 7.571$ A	$\Delta U_2 = 5.19$ V $\Delta P_2 = -787$ W	$\Delta U_4 = 4.83$ V $\Delta P_4 = 377$ W
Control point k: $s_k = 0.0274$; $I_{\mu k} = 7.135$ A; discrepancy $\Delta U_k = 0.19$ V; $\Delta P_k = 19$ W		

Note that Fig. 9 is of a general illustrative nature for the sake of clarity and does not correspond to the data in Table 5, which change with iterations.

The values of the discrepancies (33) are plotted in Fig. 9 at the corresponding points 1–4 as conditional vectors perpendicular to the coordinate plane s, I_μ.

As noted, within the coordinate rectangle 1, 2, 3, 4, a linear dependence of U_s and P_{out}, s and I_μ is allowed. Then it is possible to draw straight lines in pairs through the ends of the vectors ΔU_1 and ΔU_2, ΔU_3 and ΔU_4, and similarly through the ends of the vectors ΔP_1 and ΔP_2, ΔP_3 and ΔP_4 (see Fig. 9).

At the intersections of the formed lines with the side lines of the quadrilateral in its plane, the voltage ΔU_k and power ΔP_k deviations at points 5, 6 and 7, 8 are equal to 0. Then it is possible to write the linear equations of the formed straight lines, which are shown by a dotted line, and from these equations to determine the coordinates of the intersection points:

$$I_{\mu 5} = I_{\mu 1} - \Delta U_1 \frac{\Delta I}{\Delta U_2 - \Delta U_1};\ I_{\mu 6} = I_{\mu 1} - \Delta U_3 \frac{\Delta I}{\Delta U_4 - \Delta U_3};$$

$$I_{\mu 7} = I_{\mu 1} - \Delta P_1 \frac{\Delta I}{\Delta P_2 - \Delta P_1};\ \ I_{\mu 8} = I_{\mu 1} - \Delta P_3 \frac{\Delta I}{\Delta P_4 - \Delta P_3}.$$

Between points 5 and 6 and similarly between points 7 and 8, straight lines are drawn (in Fig. 9 these are dash-dotted lines), which have analytical expressions:

$$I_\mu = I_{\mu 5} + \frac{I_{\mu 6} - I_{\mu 5}}{\Delta s}(s - s_1); \qquad (34)$$

$$I_\mu = I_{\mu 7} + \frac{I_{\mu 8} - I_{\mu 7}}{\Delta s}(s - s_1). \qquad (35)$$

On line 5-6 $\Delta U_s = 0$, on line 7-8 $\Delta P_{out} = 0$, then at point 9 at their intersection the conditions $\Delta U_s = 0$ and $\Delta P_{out} = 0$ are fulfilled together.

From the system of linear equations (34), (35) we obtain the desired slip and magnetizing current at point k:

$$s_k = s_1 + \frac{I_{\mu 5} - I_{\mu 7}}{K_2 - K_1};\ \ I_{\mu k} = I_{\mu 7} + K_2 (s_k - s_1), \qquad (36)$$

where the coefficients $K_1 = \dfrac{I_{\mu 6} - I_{\mu 5}}{\Delta s}$; $K_2 = \dfrac{I_{\mu 8} - I_{\mu 7}}{\Delta s}$.

Substitution of the values of known quantities into these formulas gave $s_k = 0.0274$ and $I_{\mu k} = 7.135$ A, which is in Table 5.

Such values should simultaneously provide the nominal voltage U_{sN} and power P_{outN} of the TIM. To verify this, with the found values of s_k and $I_{\mu k}$, the MF is calculated using a known method and at point k, the values of voltage (14) and output power (28) are determined, respectively: $U_s = 220.19$ V and $P_{out} = 15.019$ kW. The corresponding deviations ΔU and ΔP according to (33) are only 0.19 V and 19 W, which is reflected in Table 5.

In principle, for practical design, this is already close enough to the specified nominal design parameters of the TIM U_{sN} and P_{outN}. The residual differences ΔU_s and ΔP_{out} can be explained by the fact that the functions $U_s(s, I_\mu)$ and $P_{out}(s, I_\mu)$ actually differ somewhat from the linear ones adopted in Fig. 9 and in the accompanying formulas.

To demonstrate the theoretical capability of the developed method in terms of reducing the deviations ΔU and ΔP and refining the slip s and magnetizing current I_{μ}, the iterative calculation is repeated.

But in the second iteration, the initial values of slip s_0 and current $I_{\mu 0}$ are taken as the values of s_k and $I_{\mu k}$, which are determined in the first iteration. And now the coordinate rectangle 1-2-3-4 is constructed around the new coordinate point k, and at the same time its dimensions Δs and ΔI are halved by (30, 31).

After the third iteration, the deviations at the new control point k decreased to $\Delta U_k = 0.01$ V and $\Delta P_k = 4$ W. Therefore, the further iterative process did not make sense, and the calculation results are considered final.

As a result, we obtained $s_N = 0.0274$; $I_{\mu} = I_{srs} = 7.12$ A; $I_{sN} = 29.9$ A; $I_r = 469.5$ A; $\alpha_{sr} = 83.41^{\circ}$; $M_{em} = 100$ N·m; $U_s = 220$ V; $P_{in} = 17.1$ kW; $P_{outN} = 15$ kW. That is, the calculation results of the third iteration provided sufficient refinement of the TIM design parameters. If not, it would be possible to continue the iterative calculations.

It should be noted that the presented iterative process is fully automated and its execution, together with the current MF calculations by the FEMM code, is provided by a compiled Lua script.

Thus, the numerical-field verification of the considered TIM design showed the degree of its adequacy, and here it provided its noticeable refinements. At the same time, the refinement of the power factor from 0.889 to 0.898 was revealed; efficiency from 0.875 to 0.878.

In addition, it is important that the application of the presented method to verify not very high-quality designs of other TIMs is able to detect and unacceptable errors and help correct them.

Conclusions. A theoretical basis for numerical-field support, verification and refinement of the classical design of three-phase induction motors has been formed. Based on this basis, practical calculations of their electromagnetic and energy parameters have been performed, which became possible thanks to the creation of Lua control scripts using the FEMM code.

The developed theoretical basis is strictly deterministic, despite the complexity of linear and nonlinear relationships between the structural, electromagnetic and energy parameters of the TIMs. Therefore, this basis is amenable to adequate algorithmization and programming using iterative processes.

The general structure of the theoretical basis is reinforced by a harmonic analysis of the angular and time functions of electromagnetic quantities, specifying the definition of the differential leakage resistance of the stator winding.

The developed theoretical and practical bases for checking and refining the design electromagnetic and energy parameters of the TIMs were tested on the example of its published classical design in a full cycle of calculations, which includes both the synchronous idle mode and the rated loading mode.

The results of the test showed a sufficiently high efficiency of the provided theoretical and practical bases of numerical-field calculations, which showed that the TIM design with power of 15 kW is calculated for 225 V instead of 220 V, and the output power reaches only 14.4 kW. It was determined that to reach the nominal values in the design, it is necessary to reduce the magnetizing current of the stator winding from 7.75 A to 7.12 A, and the rotor slip during operation of the TIM will have a value of 0.0274 instead of 0.0261. At the same time, such important motor parameters as torque, efficiency, power factor, stator winding current, etc. are refined.

Given the software implementation of the method of numerical-field calculations of three-phase induction motors based on the FEMM code and the Lua script, it can be built into automated methods for designing such motors.

If the output power of the designed TIM is varied, then according to the developed method and code, a family of its refined operating characteristics can be obtained in an automated calculation mode.

Conflict of interest. The author declares no conflict of interest.

REFERENCES

1. *Finite Element Method Magnetics: Download – Stable Distribution (21Apr2019) – 64-bit Executable.* Available at: https://www.femm.info/wiki/Download (Accessed: 05 May 2025).

2. Ierusalimschy R. *Reference Manual of the Programming Language Lua 4.0*. Available at: http://www.lua.org/manual/4.0/ (Accessed: 05 May 2025).

3. Goldberg O.D., Gurin Ya.S., Sviridenko I.S. *Design of electrical machines. 2nd ed., revised and additional*. Moscow, Higher School Publ., 2001. 430 p. (Rus).

4. Kopylov I.P. *Electrical machines designing*. Moscow, Yurait Publ., 2019. 828 p. (Rus).

5. Milykh V.I. Numerically-field analysis of the adequacy of the design data of three-phase induction motors and the method of their refinement on this basis. *Technical Electrodynamics*, 2018, no. 1, pp. 47-55. (Rus). doi: https://doi.org/10.15407/techned2018.01.047.

6. Milykh V.I. Numerical-field analysis of temporal functions and harmonic composition of EMF in windings of a three-phase asynchronous motor. *Technical Electrodynamics*. 2018, no. 3, pp. 56-65. (Rus). doi: https://doi.org/10.15407/techned2018.03.056.

7. Milykh V.I. The system of automated formation of electrical machines computational models for the FEMM software environment. *Technical Electrodynamics*. 2018, no. 4, pp. 74-78. (Ukr). doi: https://doi.org/10.15407/techned2018.04.074.

8. Milykh V.I. Numerical-field analysis of active and reactive winding parameters and mechanical characteristics of a squirrel-cage induction motor. *Electrical Engineering & Electromechanics*, 2023, no. 4, pp. 3-13. doi: https://doi.org/10.20998/2074-272X.2023.4.01.

9. Milykh V.I. Numerical-field analysis of differential leakage reactance of stator winding in three-phase induction motors. *Electrical Engineering & Electromechanics*, 2025, no. 2, pp. 7-18. doi: https://doi.org/10.20998/2074-272X.2025.2.02.

10. Göztaş M., Çunkaş M., Şahman M.A. In-Situ Efficiency Estimation of Induction Motors Using Whale Optimization Algorithm. *Turkish Journal of Electrical Power and Energy Systems*, 2025, vol. 5, no. 2, pp. 114-124. doi: https://doi.org/10.5152/tepes.2025.25001.

11. Michael I.N., Eneh P.I.I. Optimization of a Single-Phase Induction Motor Using Finite Element Method. *International Journal of Research Publication and Reviews*, 2025, vol. 6, no. 2, pp. 4441-4449. doi: https://doi.org/10.55248/gengpi.6.0225.1020.

12. Ding Q., Yang Z., Sun X., Zhao Q., Zhu H. Analysis of rotor slot width influence on a bearingless induction motor. *Computers & Electrical Engineering*, 2020, vol. 81, art. no. 106534. doi: https://doi.org/10.1016/j.compeleceng.2019.106534.
13. Arish N., Ardestani M., Hekmati A. Optimum Structure of Rotor Slot for a 20 kW HTS Induction Motor. *Physica C: Superconductivity and its Applications*, 2021, vol. 582, art. no. 1353829. doi: https://doi.org/10.1016/j.physc.2021.1353829.
14. Ocak C. A FEM-Based Comparative Study of the Effect of Rotor Bar Designs on the Performance of Squirrel Cage Induction Motors. *Energies*, 2023, vol. 16, no. 16, art. no. 6047. doi: https://doi.org/10.3390/en16166047.
15. Nascimento D., Smolenski R., Loschi H., Grassi F., Wan L., Hamid A. Electromagnetic Fields on 3-Phase Induction Motor Using Finite Element Analysis. *2021 IEEE International Joint EMC/SI/PI and EMC Europe Symposium*, 2021, pp. 434-439. doi: https://doi.org/10.1109/EMC/SI/PI/EMCEurope52599.2021.9559357.
16. Ding Z., Bu W., Cai X., Wu X., Liu S. Finite Element Analysis and Modeling of Three-Phase Induction Motor. *IOP Conference Series: Materials Science and Engineering*, 2019, vol. 677, no. 5, art. no. 052055. doi: https://doi.org/10.1088/1757-899X/677/5/052055.
17. Lee J.-H., Kwon Y.-C., Sul S.-K. High-Fidelity Induction Motor Simulation Model Based on Finite Element Analysis. *IEEE Transactions on Industrial Electronics*, 2022, vol. 69, no. 10, pp. 9872-9883. doi: https://doi.org/10.1109/TIE.2022.3163556.
18. Ekpo E.G. Dynamic Analysis of Two Phase Induction Motor Using Finite Element Method. *Journal of Emerging Trends in Engineering and Applied Sciences (JETEAS)*, 2020, vol. 11, no. 6, pp. 211-218. Available at: https://www.scholarlinkinstitute.org/jeteas/abstractview.php?id=6.83 (Accessed: 05 May 2025).
19. Shaier A.A., Flah A., Kraiem H., Enany M.A., Elymany M.M. Novel technique for precise derating torque of induction motors using ANFIS. *Scientific Reports*, 2025, vol. 15, no. 1, art. no. 8550. doi: https://doi.org/10.1038/s41598-025-92821-z.
20. Asaad M., Mejbel A. Losses estimation of a single - phase induction motor based on finite element analysis. *AIP Conference Proceedings*, 2023, vol. 2787, no. 1, art. no. 050019. doi: https://doi.org/10.1063/5.0148207.
21. Breivik A. *Fault Detection and Diagnosis of Induction Motor for Ship Propulsion by utilizing Electrical Signature and Finite Element Method.* Master's thesis in Marine Technology. NTNU, Norwegian University of Science and Technology, 2021, 107 p. Available at: https://ntnuopen.ntnu.no/ntnu-xmlui/handle/11250/2781526 (Accessed: 05 May 2025).
22. Babu H. *Finite-element analysis of an induction motor with inter-turn short-circuit faults.* Thesis of Master in Electrical Engineering. KTH Royal Institute of Technology, School of Electrical Engineering and Computer Science (EECS), Stockholm, Sweden, 2020, 98 p. Available at: https://urn.kb.se/resolve?urn=urn:nbn:se:kth:diva-290082 (Accessed: 05 May 2025).
23. Liang X., Ali M.Z., Zhang H. Induction Motors Fault Diagnosis Using Finite Element Method: A Review. *IEEE Transactions on Industry Applications*, 2020, vol. 56, no. 2, pp. 1205-1217. doi: https://doi.org/10.1109/TIA.2019.2958908.
24. Sakhara S., Brahimi M., Nacib L., Layadi T.M. Application of a wavelet neural network approach to detect stator winding short circuits in asynchronous machines. *Electrical Engineering & Electromechanics*, 2023, no. 3, pp. 21-27. doi: https://doi.org/10.20998/2074-272X.2023.3.03.
25. Diarra M.N., Li Y., Zhao X. Induction Motors Parameters Identification by Starting Process Using Quantum Particle Swarm Optimization-Trust Region Algorithm (QPSO-TRA). *2023 International Conference on Applied Intelligence and Sustainable Computing (ICAISC)*, 2023, pp. 1-6. doi: https://doi.org/10.1109/ICAISC58445.2023.10200090.
26. Popovych O., Golovan I. Currents System for Efficient Mathematical Modeling of an Induction Motor Using the Field Analysis. *2019 IEEE International Conference on Modern Electrical and Energy Systems (MEES)*, 2019, pp. 142-145. doi: https://doi.org/10.1109/MEES.2019.8896624.
27. Golovan I.V., Popovych O.M. Consideration of the induced current displacement in the rotor circuit in a weakly coupled circuit-field model of an induction motor. *Technical Electrodynamics*, 2025, no. 3, pp. 22-30. (Ukr). doi: https://doi.org/10.15407/techned2025.03.022.
28. Quadrado J.C. Enhancing Engineering Education: Integrating Finite Element Method Analysis for Induction Motors Efficiency Improvement Study. *Proceedings of the 22nd LACCEI International Multi-Conference for Engineering, Education and Technology: Sustainable Engineering for a Diverse, Equitable, and Inclusive Future at the Service of Education, Research, and Industry for a Society 5.0*, 2024, art. no. 2032. doi: https://doi.org/10.18687/LACCEI2024.1.1.2032.
29. Milykh V.I., Polyakova N.V. Harmonious analysis of electromagnetic sizes three-phase winding of stators of turbogenerator on basis classic and numeral field methods. *Technical Electrodynamics*, 2013, no. 3, pp. 40-49. (Rus).

Received 20.08.2025
Accepted 08.11.2025
Published 02.01.2026

V.I. Milykh[1], *Doctor of Technical Science, Professor,*
[1] National Technical University «Kharkiv Polytechnic Institute», 2, Kyrpychova Str., Kharkiv, 61002, Ukraine,
e-mail: mvikemkpi@gmail.com

How to cite this article:
Milykh V.I. Theory and practice of numerical-field analysis and refinement of electromagnetic and energy parameters in the designs of three-phase induction motors. *Electrical Engineering & Electromechanics*, 2026, no. 1, pp. 3-14. doi: https://doi.org/10.20998/2074-272X.2026.1.01